ADVANCED MATERIALS INTERFACES
Open Access
www.advmatinterfaces.de

Ultra-Flexible Giant Magnetoresistance Biosensors for Lab-on-a-Needle Biosensing

Diqing Su, Kai Wu, Karthik Srinivasan, Zohreh Nemati, Reza Zamani, Vinit Chugh, Renata Saha, Rhonda Franklin, Jaime Modiano, Bethanie Stadler, and Jian-Ping Wang**

Flexible biosensors exhibit great potential for the detection of various biomarkers with the ability to adapt to different surface textures. Here, a lab-on-a-needle biosensing platform based on ultra-flexible giant magnetoresistance (GMR) biosensors is developed. The fabricated flexible GMR sensors exhibit a MR ratio of 5.2% and a sensitivity of 0.13%/Oe in the linear region, which are comparable to their rigid counterparts. It is found that the magnetic properties of the flexible GMR sensors remain unchanged after 500 cycles of compressive and tensile stress, indicating strong robustness even when applied to a surface that is constantly in motion. The developed platform is then employed for the detection of different concentrations of canine osteosarcoma (OSCA-8) cells with a limit of detection (LOD) of 200 cells in 20 μL sample (10^4 cells per mL), which demonstrate the ability to perform real-time, sensitive, and quantitative cell detection.

1. Introduction

Flexible electronics have attracted tremendous attention in the past few years due to their capability of altering geometries on complex surfaces or under multiple stress cycles while maintaining the device performance.[1–5] Flexible electronics have been used in various applications such as artificial intelligent skins,[6,7] which can monitor the heat, texture, pressure, and strain of the surrounding environment, and stretchable lithium-ion batteries,[8] which serve as the power supply in an all-flexible circuit. In the field of sensing, sensors that can deform with biological surfaces, such as skins and organs, are desirable to obtain more reliable and more accurate information, and flexible biosensors are promising candidates for such applications. Recently, flexible biosensors with various mechanisms have been developed including electrochemical sensors,[9,10] plasmonic sensors,[11,12] piezoelectric sensors,[13,14] etc., for the detection of small molecules,[15,16] proteins,[17] nucleic acids,[18] as well as bacteria.[19]

Although electrochemical and optical biosensors have been widely employed, their sensor signal can be influenced by the sample matrix, especially in complex biological fluids. On the contrary, magnetoresistance (MR) biosensors utilize the

D. Su, B. Stadler, J.-P. Wang
Department of Chemical Engineering and Materials Science
University of Minnesota
Minneapolis, MN 55455, USA
E-mail: stadler@umn.edu; jpwang@umn.edu

K. Wu, K. Srinivasan, Z. Nemati, R. Zamani, V. Chugh, R. Saha, R. Franklin, B. Stadler, J.-P. Wang
Department of Electrical and Computer Engineering
University of Minnesota
Minneapolis, MN 55455, USA

R. Franklin, B. Stadler, J.-P. Wang
Masonic Cancer Center
University of Minnesota
Minneapolis, MN 5455, USA

The ORCID identification number(s) for the author(s) of this article can be found under https://doi.org/10.1002/admi.202201417.

DOI: 10.1002/admi.202201417

R. Franklin, J. Modiano, B. Stadler, J.-P. Wang
Institute for Engineering in Medicine
University of Minnesota
Minneapolis, MN 55455, USA

J. Modiano
Animal Cancer Care and Research Program
University of Minnesota
St. Paul, MN 55108, USA

J. Modiano
Department of Veterinary Clinical Sciences
College of Veterinary Medicine
University of Minnesota
St. Paul, MN 55108, USA

J. Modiano
Center for Immunology
University of Minnesota
Minneapolis, MN 55455, USA

J. Modiano
Stem Cell Institute
University of Minnesota
Minneapolis, MN 55455, USA

magnetic field from magnetic labels as the source of the sensor signal. Since most biological samples are nonmagnetic, a lower background noise can be expected for MR sensors compared to optical and electrochemical sensors.[20–22] Flexible MR sensors can be fabricated through several different approaches, such as direct deposition on flexible substrates,[23,24] transfer of devices from rigid substrates to flexible substrates,[25] and backside thinning of substrates.[26,27] Despite these investigations on fabrication technologies, flexible MR sensors have yet to be used in biological detection due to the limited sensor sensitivity, high noise in flexible detection systems, and the lack of effective signal processing approaches.

Biosensors on flexible substrates have facilitated the possibility of integrating sensing devices with various medical tools, such as needles, which can be employed in real-time, in situ monitoring of the disease conditions, locating the surgical sites of interest, and studying biological models in vitro. With the ultra-flexible substrates, the biosensors can be integrated at the tip of the medical tools without interfering their original functions, which is called a lab-on-a-needle platform. Compared with other kind of platforms, the lab-on-a-needle platform has attracted much attention due to its capability of continuous detection for the target biomolecules in a fairly localized region during in vivo or in vitro medical procedures. Several attempts have been made to fabricate biosensors on needle-shaped medical tools either by the direct fabrication of biosensors with the needle serving as part of the sensing device,[28] or by fabricating flexible sensors and attaching them to the surface of a needle.[9] However, most of the demonstrated approaches were based on electrochemical sensors and focused on the detection of the chemical environment or small molecules. In addition to molecular-level detection, the direct detection of whole cells is also necessary. Here, a lab-on-a-needle sensing platform based on giant magnetoresistance (GMR) sensors was developed. The potential of employing this platform for real-time, sensitive, and quantitative cell detection was validated through the detection of cultured canine osteosarcoma cells (OSCA-8 cell line[29]) with magnetic nanowires (MNWs) as labels.

2. Experimental Section

2.1. Fabrication of Flexible GMR Sensors

The fabrication process of flexible GMR sensors is shown in **Figure 1**a. GMR stacks with the structure of Ta(5)/IrMn(8)/CoFe(2.5)/Cu(2.8)/CoFe(1)/NiFe(2)/Ta(5) (in nm) were first

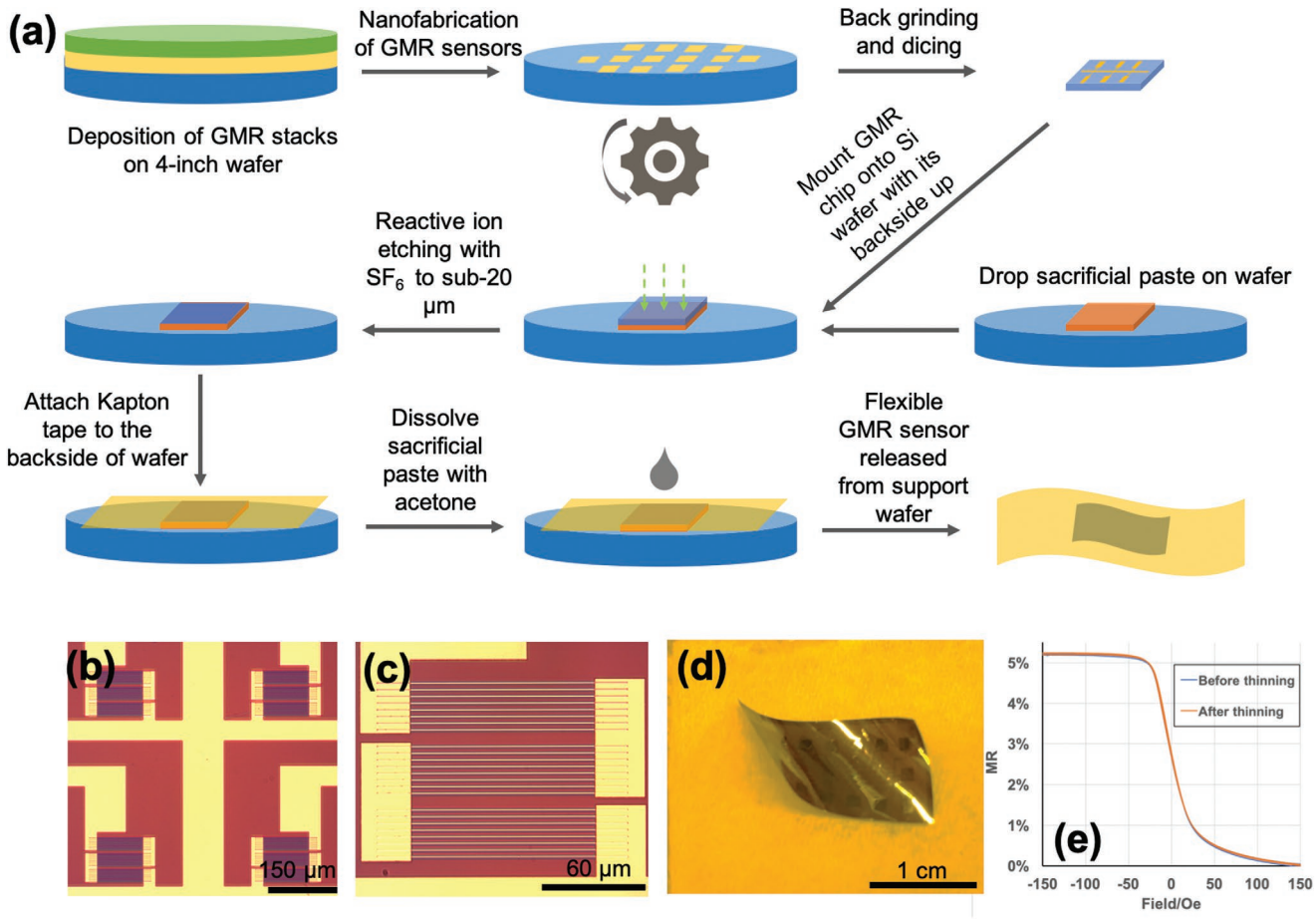

Figure 1. a) Schematic illustration of the fabrication process for the flexible GMR sensors. Optical microscope image of b) the sensor arrays and c) one single sensor on the flexible GMR chip. d) Image of the backside of a free-standing flexible GMR chip. The ultra-thin Si membrane became transparent, making it possible to visualize the sensor arrays on the frontside. e) MR-H curves of the GMR chip before and after backside thinning.

prepared on 4 in. Si/SiO_2 wafers by magnetron sputtering, followed by the definition of the sensor area and the formation of electrical contacts through nanofabrication. The sensor surface is covered with SiO2 for passivation. The fabricated GMR wafers were back-polished with a diamond-resin bonded grinding wheel to a thickness of 50 μm. The wafers were then diced into individual GMR chips for subsequent processing. The GMR chips were annealed under a magnetic field of 5000 Oe at 200 °C for 1 h to fix the magnetization direction of the pinned layer to the short axis of the GMR sensors. The thickness of the chip was then further reduced through reactive ion etching (RIE), where the chip was mounted on a support silicon wafer via a thermal conductive paste. The thermal conductive paste also served as the sacrificial layer for the release of the etched chip. After etching with SF_6 for 15 min, the thickness of the chip was reduced to sub-20 μm. Kapton tape was attached to the back of the GMR chip, followed by an acetone wash to dissolve the thermal conductive paste, thereby releasing the flexible GMR chip from the support wafer. It should be noted that this transfer method is universal. The GMR sensors can be transferred to other substrates that are more stretchable or adhesive than Kapton tapes, such as PDMS, based on the applications. Optical images of the fabricated flexible GMR chip are shown in Figure 1b,c. There were 14 GMR sensors on each chip. One individual GMR sensor consisted of 24 high-aspect-ratio stripes with the dimension of 150 μm × 0.75 μm. The whole chip has an area of ≈3 cm^2. As shown in Figure 1d, the released GMR chip exhibited high flexibility while maintaining the nanofabricated patterns in their rigid counterparts. The back-etching method demonstrated here had several advantages compared to the previously reported flexible GMR sensor fabrication technology, where GMR stacks were deposited directly on flexible substrates.[25,30] The crystal structure and interfaces of magnetic thin films, and therefore GMR performance, were highly influenced by the surface roughness and the mechanical properties of the substrate. GMR stacks deposited onto rigid Si yield high quality crystal structures and interfaces, unlike GMR stacks that were deposited onto flexible substrates, and these qualities were maintained during the thinning process, as suggested by the almost unchanged magnetoelectric response of the devices after backside thinning (Figure 1e). In addition, the nanofabrication process based on the back-etching method was performed on standard Si wafers, which eliminated the need of designing new fabrication processes for flexible substrates, making it easier to realize mass production.

2.2. Preparation of MNW-Cell Samples

Ni magnetic nanowires (MNWs) were fabricated through electrochemical deposition into anodic aluminum oxide (AAO) templates. Briefly, 7 nm Ti and 200 nm Cu were first sputter deposited on the bottom side of the AAO templates as the adhesion layer and the electrode for the subsequent electrochemical deposition, respectively. The electrolyte contained nickel sulfate, nickel chloride, and boric acid with the pH adjusted to 4.5 by the addition of diluted NaOH. The Ni MNWs had diameters (120 nm) matched with the pores of the template.

To label cells with MNWs, 10^6 canine OSCA-8 cells were incubated for 18 h in in DMEM medium supplemented with 10% FBS.[31] The propagated cells were then placed into each well of a 6-well plate, followed by another 18 h of incubation in the same medium. The Ni MNWs were functionalized in 0.5 M NaCl solution containing 1 mg PEG/mg Ni at pH ≈ 13 for 24 h at 4 °C. Subsequently, the Ni MNWs were incubated with the OSCA-8 cells for 48 h, during which time the Ni MNWs were internalized by the cells. After incubation, the cells were fixed with a mixture of 2.5% glutaraldehyde and 0.1 M Cacodylate for 50 min, rinsed three times with 0.1 M sodium cacodylate, and dehydrated in ethanol. Since this work is a proof-of-concept demonstration, fixed cells were used to avoid any uncontrollable contribution from the biochemical reactions within the cells. But in principle, the detection of live cells can be performed in the same manner. Extra MNWs were washed away before the cells were detached from the glass with trypsin to avoid their contribution to the noise of the sensor. Finally, the fixed Ni-MNW-OSCA-8 cells were magnetically separated from the assay and re-suspended in water for subsequent biological detection processes (**Figure 3**a–d). Both MNWs and MR sensors demonstrated minimal cytotoxicity according to previous works.[32–34]

3. Results and Discussions

3.1. Magnetic Properties of Flexible GMR Sensors

The fabricated flexible GMR sensors were attached to the surfaces of customized rods with bending radius (r) of 10, 5, and 1 mm (**Figure 2**a–c). The MR response of the sensors for each bending radius was recorded under the magnetic field ranging from −180 to 180 Oe (Figure 2d). The MR curve of a flat sensor was also shown as a control experiment. An MR ratio of 5.2% was obtained for the flat chips, with an MR ratio of 3.4% in the linear region (−30 to 30 Oe), which was comparable to the previously reported results.[35,36] All of the MR response curves exhibited negligible hysteresis, which was crucial for biosensing applications since the sensor signal should be independent of the history of the applied magnetic field, meaning only one amplitude of sensor signal should be correlated to each target concentration in the calibration curve. As the bending radius decreased from 10 to 1 mm, both the MR ratio and the slope in the linear region (S) decrease, as shown in Figure 2e, which can be attributed to the increase of the anisotropy field from the permalloy layer due to the magnetoelastic effect. Note that the sensitivity was calculated by the slope of the RH curve in the linear region ($\Delta MR/\Delta H$), as shown in the inset of Figure 2d, where H is the magnetic field. This observation was consistent with earlier studies which demonstrated that the anisotropy field of a permalloy film is proportional to its curvature.[37–39] It is worth noting that the MR ratio only dropped 0.2% from 5.2% for flat chip to 5.0% at $r = 1$ mm, indicating that the MR value was almost independent of the bending radius. On the contrary, more than 30% drop in S was observed as the bending radius decreased, which should be considered as a key factor in the process of designing flexible MR biosensors. In addition, the robustness of the devices was also evaluated through a series of

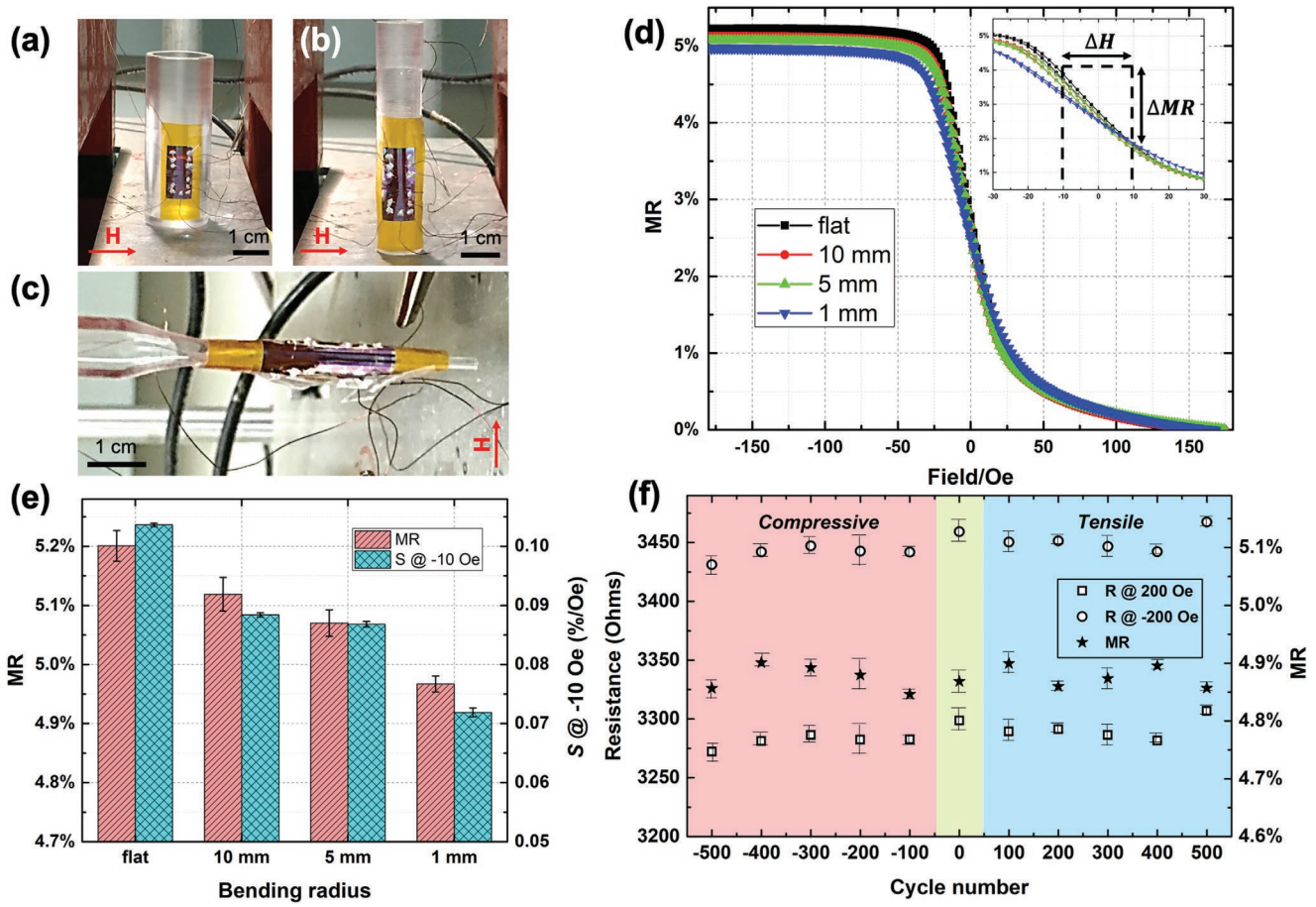

Figure 2. The experimental setup for the RH loop measurement of the flexible GMR sensors under bending radius of a) 10, b) 5, and c) 1 mm. Magnetic field directions are denoted by the red arrows. d) The RH curves of the GMR sensors under different bending radius. The RH curves in the linear region are shown in the inset. e) The influence of bending radius on the MR ratio and the sensitivity (*S*) of the GMR sensors. f) Resistance and MR ratio of flexible GMR sensors under compressive stress (0 to −500 cycles) and tensile stress (0 to 500 cycles).

fatigue tests. During the test, the flexible devices went through 500 identical bending cycles at a bending radius of 1 mm under both tensile and compressive stress. The tensile and compressive strain associated with the bending process is around 10% based on the Young's modulus and the thickness of the Kapton tape. As shown in Figure 2f, both the resistance change and the MR change were within 1.5% throughout the entire test, indicating highly reproducible magnetic properties of these flexible sensors as well as the robustness of the device under a large amount of workload.

3.2. Characterization of Ni-MNW-OCSA-8 Cells

The preparation process of Ni-MNW-OCSA-8 cells was shown in Figure 3a–d. The shape and size of these synthesized Ni MNWs were then characterized by scanning electron microscopy (SEM) and energy-dispersive X-ray spectroscopy (EDS) (Figure 3e,f). As shown in Figure 3g, the MNWs have uniform lengths of 1 µm. The energy-dispersive X-ray spectroscopy (EDS) analysis (Figure 3h) confirmed the presence of Ni from the MNWs in the imaged region. The other peaks shown in the EDS data mainly originate from the SiO_2 and Al_2O_3 passivation layers on the sensor surface. Next, 20 µL of Ni-MNW-OCSA-8 cells were dropped on the GMR sensor surface for further characterization. After the water fully evaporated, the Ni-MNW-OSCA-8 cells on the GMR sensor surface (shown in Figure 3i,j) were observed, and their diameters were estimated to be 10–20 µm. The actual size of the cells before fixation was 35–40 µm in diameter. No MNWs were observed outside the cells. This means that all the stray field sensed by the GMR sensors originated from MNWs internalized by the tumor cells, which was consequently proportional to the cell concentrations. The total number of cells on each sensor surface was calculated based on the average number of cells located on one GMR sensor stripe and the ratio between the area of one sensor and the total area of the sample spot. The concentration of cells in the sample can be further estimated based on the volume of the sample spotted on the sensor, namely 2×10^5 cells per mL.

3.3. Cell Detection with Flexible GMR Sensors

Flexible GMR sensors on a biopsy needle can serve as a tool for the in situ identification of tumor cells at potential tumor sites. A schematic illustration of the detection principle is

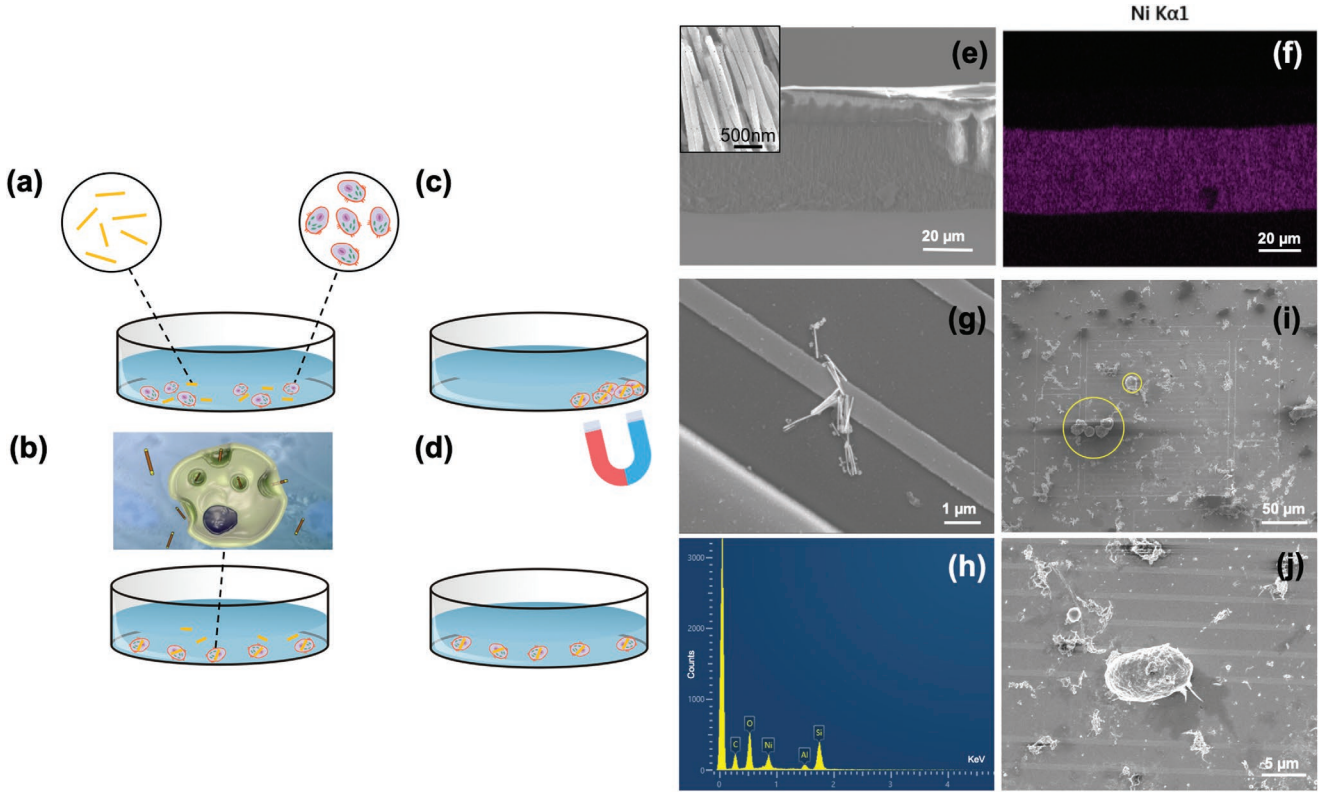

Figure 3. a–d) Schematic illustration of the preparation process of Ni-MNW-OCSA-8 cells. The cells were first incubated with Ni MNWs (a). After the MNWs were internalized by the cells (b), the unattached MNWs were washed away while the cells were attached to the bottom of the petri dish. The cells were then detached from the glass with trypsin, separated by magnet (c) and re-dispersed in PBS (d). e) SEM image of Ni MNWs grown in the AAO template (inset: zoom-in image of the MNWs). f) EDS analysis of the Ni MNWs grown in the AAO template. g) The SEM image of Ni MNW clusters on one GMR sensor stripe. h) EDS data for the MNW cluster shown in (e). i) SEM image of Ni-MNW-OSCA-8 cells on sensor surface. Cell positions are highlighted in yellow circles. j) SEM image of one Ni-MNW-OSCA-8 under higher magnification.

shown in **Figure 4**a. Although this study involved non-specific uptake, MNWs can be labeled for specific internalization into tumor cells.[34] The magnetic field from the MNWs within the tumor cells can be detected by the GMR sensors at the tip of the biopsy needle. To validate the potential of the current platform for such application, OSCA-8 cell detection based on flexible GMR sensors was performed using the bending radius of 1 mm, which was realized by wrapping the GMR chip around the tip of a glass needle (Figure 4b). During the detection, the needle was inserted into a reaction tube. Upon addition of 20 μL Ni-MNW-cell samples into the tube, the stray field from the MNWs induced a resistance change in the GMR sensors, resulting in the change of the RH loops (Figure 4c). Since the number of MNWs existing in the sample was proportional to the concentration of target cells, the sensor signals increased as the cell concentration increased, realizing quantitative detection of cell samples. The sensor signal was analyzed via two methods: full-loop MR response measurements and real-time resistance measurements.

In the full-loop measurement, the RH curves of the GMR sensors were scanned under an external magnetic field from –100 to 100 Oe before and after the addition of cell samples. The RH curves of the GMR sensors in the field range of –100 to 100 Oe are shown in Figure 4d. Six different cell concentrations were employed for detection, ranging from 4.4×10^4 to 4×10^5 cells per mL. Two negative control groups were measured in parallel. Specifically, for one group of GMR sensors, 20 μL of PBS was added to the reaction tube (0 cells per mL), and for the other group, nothing was added to the reaction tube. As the cell concentration increased, distinctive changes in the RH loops were observed. The change of RH loops can be attributed to the effective field (H_{eff}) generated by the MNWs as shown in Figure 4c. As H_{eff} was always in the opposite direction to the applied magnetic field (H_a), the resistance of the GMR sensor at H_a with the cell sample should be equivalent to the resistance of the GMR sensor at $H_a - H_{eff}$. Consequently, the slope of the RH loop in the linear region should decrease with the increase of the effective field, which was proportional to the cell concentrations (Figure 4d). As expected, the calculated effective field increased linearly with the cell concentration, from 2.9 Oe at 4.4×10^4 cells per mL to 18.32 Oe at 4×10^5 cells per mL (Figure 4e). The effective field generated per cell was thus calculated to be 2.5×10^{-3} Oe considering a sample volume of 20 μL. The sensor signal for the full-loop measurement can be explicitly expressed either in the form of the MR value at saturation field or the slope of the response curve at 0 Oe, both of which decreased linearly with increased cell concentrations (Figure 4f,g).

In addition to the full-loop measurement, the real-time monitoring of Ni-MNW-cells landing on GMR sensors was

ADVANCED MATERIALS INTERFACES
Open Access
www.advmatinterfaces.de

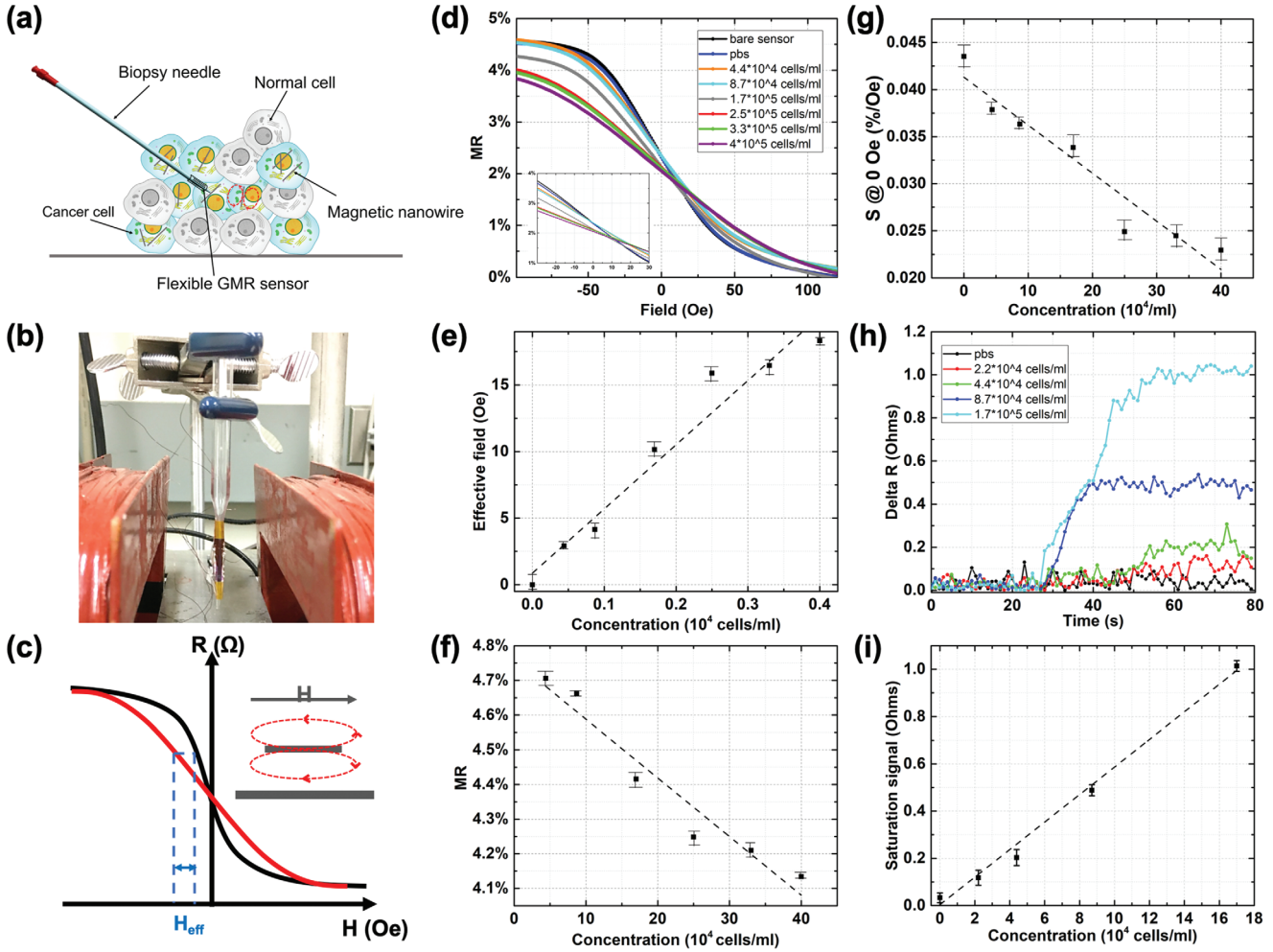

Figure 4. a) Schematic illustration of the detection principle for tumor cell identification at potential tumor sites with lab-on-a-needle flexible GMR biosensors. b) Images of the experimental setup for lab-on-a-needle detection of OSCA-8 cells. c) Schematic illustration of the stray field from the MNWs near sensor surface and the RH loops before (black) and after (red) the addition of Ni-MNW-cells. d) MR response curve of flexible GMR sensors under different cell concentrations. The inset exhibits the response curves within the linear region. e–g) Cell concentration dependence of e) effective field, f) MR, and g) Sensitivity during full-loop measurement. h) Real-time sensor signal under different concentrations. i) Calibration curve of the saturation signal at different cell concentrations.

also demonstrated, where the resistance of the GMR sensors was recorded under a constant applied field of 10 Oe to bias the sensor in the linear region of the MR response. The baseline was first acquired for 20 s, followed by the addition of the cell samples. As shown in Figure 4h, the resistance change (ΔR) increased as the cell samples were added to the reaction tube due to the induced MNW stray field and saturated when the movement of the cells near sensor surface reached equilibrium. The fluctuation of the sensor signal after saturation originated from the noise of the detection system as well as the motion of the cells. A linear relationship was observed between the cell concentration and the saturated sensor signal, indicating the capability of quantitative, real-time detection of cells based on the flexible GMR sensors (Figure 4i). The limit of detection (LOD) of the system was calculated as the cell concentrations with the sensor signal twice as large as the noise level. A LOD of 10^4 cells per mL was realized based on the real-time detection data, which corresponds to 200 cells in the sample. The sensor performance can be further improved by optimizing the electronics within the platform, as well as the employment of surface biofunctionalization techniques for cell detection through chemical bonding. It is important to realize that this detection was done for a sample volume of 20 µL or 20mm^3 (4.5 mm × 4.5 mm × 4.5 mm), which is about the size of a small lymph node.

4. Conclusions

In this work, flexible GMR biosensor arrays were fabricated with a two-step backside thinning approach. The GMR sensors were first fabricated on Si substrates followed by the mechanical grinding and RIE processes, resulting in sensor arrays on a Si membrane with sub-20 µm thickness. The fabricated GMR sensors exhibited ultra-high flexibility, strong robustness under multiple bending cycles, and comparable MR ratios and

sensitivities to their rigid counterparts under different bending radius. A lab-on-a-needle sensing platform was developed by attaching the ultra-flexible GMR sensors to the tip of a glass needle with a radius of 1 mm. Despite the tight bending curvature, the detection of OSCA-8 cells was performed successfully. Two different sensor signal acquisition approaches were employed during the detection. The sensor signal can be expressed as the MR ratio, the slope of response curve in the linear region, as well as the effective field in the full-loop measurement. Real-time measurement was also realized by biasing the magnetic sensors to the linear operation region with a constant magnetic field, where a LOD of 10^4 cells per mL was achieved, corresponding to 200 cells in the sample. Sensor signals from both the full loop measurement and the real-time measurement exhibited great linearity with cell concentrations, demonstrating the platform's great potential in real-time, sensitive, and quantitative cell detection.

5. Statistics

All the presented data in this manuscript is processed by Origin. No additional pre-processing of the data is employed unless specified in the main text. The error bars in the plots are calculated by the standard deviation of the data from 14 sensors in the sensor array.

Acknowledgements

This study was financially supported by the Institute of Engineering in Medicine of the University of Minnesota through FY18 IEM Seed Grant Funding Program. This study was also financially supported by the U.S. Department of Agriculture – National Institute of Food and Agriculture (NIFA) under Award Number 2020-67021-31956. The authors acknowledge the MAF grant (D15CA-047) and the grant from the Skippy Frank Fund for Life Sciences and Translational Research. Portions of this work were conducted in the Minnesota Nano Center, which is supported by the National Science Foundation through the National Nano Coordinated Infrastructure Network (NNCI) under Award Number ECCS-1542202. Portions of this work were carried out in the Characterization Facility, University of Minnesota, a member of the NSF-funded Materials Research Facilities Network (www.mrfn.org) via the MRSEC program.

Conflict of Interest

Competing interests: Dr. Jian-Ping Wang has equity and royalty interests in, and serves on the Board of Directors, for Zepto Life Technology LLC, a company involved in the commercialization of GMR Biosensing technology. The University of Minnesota also has equity and royalty interests in Zepto Life Tech LLC. These interests have been reviewed and managed by the University of Minnesota in accordance with its Conflict of Interest policies. All the other authors declare no conflict of interest.

Data Availability Statement

The data that support the findings of this study are available from the corresponding author upon reasonable request.

Keywords

biosensor, cell detection, flexible, magnetic nanowire, magnetoresistance

Received: June 26, 2022
Revised: November 12, 2022
Published online: January 12, 2023

[1] Y. Ma, Y. Zhang, S. Cai, Z. Han, X. Liu, F. Wang, Y. Cao, Z. Wang, H. Li, Y. Chen, X. Feng, *Adv. Mater.* **2020**, *32*, 1902062.
[2] P. Wang, M. Hu, H. Wang, Z. Chen, Y. Feng, J. Wang, W. Ling, Y. Huang, *Adv. Sci.* **2020**, *7*, 2001116.
[3] J. Wan, J. Xie, X. Kong, Z. Liu, K. Liu, F. Shi, A. Pei, H. Chen, W. Chen, J. Chen, X. Zhang, L. Zong, J. Wang, L.-Q. Chen, J. Qin, Y. Cui, *Nat. Nanotechnol.* **2019**, *14*, 705.
[4] S. Lee, D. Sasaki, D. Kim, M. Mori, T. Yokota, H. Lee, S. Park, K. Fukuda, M. Sekino, K. Matsuura, T. Shimizu, T. Someya, *Nat. Nanotechnol.* **2019**, *14*, 156.
[5] T. Leydecker, M. Herder, E. Pavlica, G. Bratina, S. Hecht, E. Orgiu, P. Samori, *Nat. Nanotechnol.* **2016**, *11*, 769.
[6] D. Li, W.-Y. Lai, Y.-Z. Zhang, W. Huang, *Adv. Mater.* **2018**, *30*, 1704738.
[7] Y. Gong, Y.-Z. Zhang, S. Fang, C. Liu, J. Niu, G. Li, F. Li, X. Li, T. Cheng, W.-Y. Lai, *Appl. Phys. Rev.* **2022**, *9*, 021403.
[8] S. Wang, J. He, Q. Li, Y. Wang, C. Liu, T. Cheng, W.-Y. Lai, *Fundam. Res.* **2022**, https://doi.org/10.1016/j.fmre.2022.06.003.
[9] J. Park, J. R. Sempionatto, J. Kim, Y. Jeong, J. Gu, J. Wang, I. Park, *ACS Sens.* **2020**, *5*, 1363.
[10] M. Xu, V. K. Yadavalli, *ACS Sens.* **2019**, *4*, 1040.
[11] J. Zhu, Z. Wang, S. Lin, S. Jiang, X. Liu, S. Guo, *Biosens. Bioelectron.* **2020**, *150*, 111905.
[12] S. Mohapatra, R. S. Moirangthem, *Sens. Actuators, B* **2019**, *301*, 127070.
[13] Y. Mao, W. Zhang, Y. Wang, R. Guan, B. Liu, X. Wang, Z. Sun, L. Xing, S. Chen, X. Xue, *Sci. Adv. Mater.* **2019**, *11*, 351.
[14] Z. H. Mo, X. H. Long, W. L. Fu, *Anal. Commun.* **1999**, *36*, 281.
[15] M. Mathew, S. Radhakrishnan, A. Vaidyanathan, B. Chakraborty, C. S. Rout, *Anal. Bioanal. Chem.* **2021**, *413*, 727.
[16] Y. Cai, B. Liang, S. Chen, Q. Zhu, T. Tu, K. Wu, Q. Cao, L. Fang, X. Liang, X. Ye, *Biosens. Bioelectron.* **2020**, *165*, 112408.
[17] S. Sivashankar, C. Sapsanis, U. Buttner, K. N. Salama, *Electron. Lett.* **2015**, *51*, 1746.
[18] J. Gao, Y. Gao, Y. Han, J. Pang, C. Wang, Y. Wang, H. Liu, Y. Zhang, L. Han, *ACS Appl. Electron. Mater.* **2020**, *2*, 1090.
[19] Y. Wang, J. Ping, Z. Ye, J. Wu, Y. Ying, *Biosens. Bioelectron.* **2013**, *49*, 492.
[20] J. Schotter, P. B. Kamp, A. Becker, A. Puhler, G. Reiss, H. Bruckl, *Biosens. Bioelectron.* **2004**, *19*, 1149.
[21] R. Weiss, R. Mattheis, G. Reiss, *Meas. Sci. Technol.* **2013**, *24*, 17.
[22] B. Srinivasan, Y. Li, Y. Jing, Y. Xu, X. Yao, C. Xing, J.-P. Wang, *Angew. Chem., Int. Ed.* **2009**, *48*, 2764.
[23] D. Makarov, M. Melzer, D. Karnaushenko, O. G. Schmidt, *Appl. Phys. Rev.* **2016**, *3*, 011101.
[24] H. Li, Q. Zhan, Y. Liu, L. Liu, H. Yang, Z. Zuo, T. Shang, B. Wang, R.-W. Li, *ACS Nano* **2016**, *10*, 4403.
[25] M. Melzer, D. Karnaushenko, G. Lin, S. Baunack, D. Makarov, O. G. Schmidt, *Adv. Mater.* **2015**, *27*, 1333.
[26] J.-Y. Chen, Y.-C. Lau, J. M. D. Coey, M. Li, J.-P. Wang, *Sci. Rep.* **2017**, *7*, 42001.
[27] C. Yin, D. Xie, J.-L. Xu, T.-L. Ren, *Mod. Phys. Lett. B* **2014**, *28*, 1450081.
[28] N. Arroyo-Curras, J. Somerson, P. A. Vieira, K. L. Ploense, T. E. Kippin, K. W. Plaxco, *Proc. Natl. Acad. Sci. U. S. A.* **2017**, *114*, 645.
[29] M. C. Scott, A. L. Sarver, K. J. Gavin, V. Thayanithy, D. M. Getzy, R. A. Newman, G. R. Cutter, K. Lindblad-Toh, W. C. Kisseberth,

L. E. Hunter, S. Subramanian, M. Breen, J. F. Modiano, *Bone* **2011**, *49*, 356.
[30] M. Melzer, G. Lin, D. Makarov, O. G. Schmidt, *Adv. Mater.* **2012**, *24*, 6468.
[31] C. M. Cannon, J. Pozniak, M. C. Scott, D. Ito, B. H. Gorden, A. J. Graef, J. F. Modiano, *Vet. Comp. Oncol.* **2015**, *13*, 48.
[32] L. P. Felix, J. E. Perez, M. F. Contreras, T. Ravasi, J. Kosel, *Toxicol. Rep.* **2016**, *3*, 373.
[33] D. Moretti, M. L. DiFrancesco, P. P. Sharma, S. Dante, E. Albisetti, M. Monticelli, R. Bertacco, D. Petti, P. Baldelli, F. Benfenati, *Front. Neurosci.* **2018**, *12*, 909.
[34] A. Sharma, G. M. Orlowski, Y. Zhu, D. Shore, S. Y. Kim, M. D. DiVito, A. Hubel, B. J. H. Stadler, *Nanotechnology* **2015**, *26*, 135102.
[35] K. Wu, T. Klein, V. D. Krishna, D. Su, A. M. Perez, J.-P. Wang, *ACS Sens.* **2017**, *2*, 1594.
[36] D. Su, K. Wu, V. D. Krishna, T. Klein, J. Liu, Y. Feng, A. M. Perez, M. C.-J. Cheeran, J.-P. Wang, *Front. Microbiol.* **2019**, *10*, 1077.
[37] C. Gudeman, *IEEE Trans. Magn.* **1990**, *26*, 2580.
[38] M. P. Hollingworth, M. R. J. Gibbs, S. J. Murdoch, *J. Appl. Phys.* **2003**, *94*, 7235.
[39] N. Perez, M. Melzer, D. Makarov, O. Ueberschaer, R. Ecke, S. E. Schulz, O. G. Schmidt, *Appl. Phys. Lett.* **2015**, *106*, 153501.